AIAA JOURNAL
Vol. 40, No. 8, August 2002

Transition Prediction for Three-Dimensional Boundary Layers in Computational Fluid Dynamics Applications

J. D. Crouch,* I. W. M. Crouch,† and L. L. Ng‡
Boeing Commercial Airplane Group, Seattle, Washington 98124-2207

A method is presented for estimating the laminar/turbulent transition location in three-dimensional boundary layers for computational fluid dynamics (CFD) applications requiring numerous transition estimates with no user intervention. Given the Reynolds number and the C_P distribution, the location of transition is estimated based on the attachment-line state, the potential for relaminarization, the occurrence of laminar separation, and the growth of instabilities. Transition caused by instability is estimated based on N factors calculated for Tollmien–Schlichting waves and for stationary crossflow instabilities. A neural network is used (in place of solving the Orr–Sommerfeld stability equation) for determining the instability growth rates. The current version of the method assumes incompressible flow. The boundary-layer flow and instabilities are calculated based on an infinite-sweep (strip boundary layer) approximation; the instability calculations also employ the parallel-flow approximation. Comparisons with traditional stability codes show good N-factor agreement over a practical range of C_P distributions. The method is several hundred times faster than traditional stability calculations, and it is robust enough to function as a simple "subroutine" in CFD codes. The method is biased toward application efficiency and simplicity as balanced against improvements in the detailed physical modeling.

Nomenclature

A	=	amplitude of instability
A_0	=	initial amplitude of instability at the neutral point
C	=	reference wing chord
C_p	=	pressure coefficient
E_{ave}	=	average error of the neural network based on the entire training set
e^N	=	A/A_0; amplitude ratio of instability
F	=	$10^6\omega\nu/Q_e^2$; dimensionless frequency parameter
g	=	scaled growth rate
g_j	=	scaled growth rate output from neutral network
J	=	number of conditions used in the neural-network training set
K	=	$(\nu/Q_e^2)\,\mathrm{d}Q_e/\mathrm{d}x_s$; relaminarization parameter
N^*	=	correlated value of N at which transition occurs
Q_e	=	boundary-layer edge velocity
Q_∞	=	freestream velocity
$\bar{R}$	=	$W_e/\sqrt{(\nu\,\mathrm{d}U_e/\mathrm{d}x|_{x=0})}$; attachment-line Reynolds number
R_C	=	$Q_\infty C/\nu$; chord Reynolds number
U, V, W	=	boundary-layer velocity in x, y, z
U_s, W_s	=	boundary-layer velocity in x_s, z_s
u, v, w	=	instability eigenfunction in x, y, z
X, Y	=	coordinate system of a wing section cut; X is in the freestream direction
x	=	chordwise coordinate (Fig. 1)
x_s, y, z_s	=	streamwise coordinate system; x_s is streamwise
y	=	distance normal to surface
z	=	spanwise coordinate
α	=	complex chordwise wave number
β	=	real spanwise wave number
β_H	=	Hartree parameter for Falkner–Skan boundary layer
γ	=	maximum growth rate over β [Eq. (2.3)]
δ_1^*	=	$\displaystyle\int_0^\infty \left(1 - \frac{U_s}{Q_e}\right)\mathrm{d}y$ displacement thickness based on U_s profile
δ_2^*	=	$\displaystyle\int_0^\infty \left(\frac{W_s}{Q_e}\right)\mathrm{d}y$ thickness based on W_s profile
Λ	=	wing sweep
ν	=	kinematic viscosity
ψ_e	=	$\tan^{-1}(W_e/U_e)$; inviscid streamline angle
ω	=	real frequency

Subscripts

CF	=	crossflow instability
e	=	value at boundary-layer edge
TS	=	Tollmien–Schlichting instability
∞	=	freestream condition

Received 23 April 2001; presented as Paper 2001-2989 at the AIAA 31st Fluid Dynamics Conference, Anaheim, CA, 11–14 June 2001; revision received 20 January 2002; accepted for publication 30 January 2002.

*Associate Technical Fellow, Acoustics and Fluid Mechanics.
†Contractor, Aerodynamics Research.
‡Principal Engineer, Acoustics and Fluid Mechanics.

I. Introduction

IMPROVEMENTS in computer power, grid-generation methods, and solution algorithms are enabling increasingly complicated applications of computational fluid dynamics (CFD). This, in turn, is putting increasing demands on the models used for capturing the unresolved flow physics. This is particularly evident in the calculation of separated flows. The location of separation has a global effect on the flowfield that can significantly alter integral quantities such as lift, drag, and pitching moment. The location of separation depends on the upstream history of the boundary layer. Prediction of this location is sensitive to the modeling of turbulence and the prediction of the laminar/turbulent transition location.

One example of an application area that has demonstrated strong sensitivity to transition is high-lift design. Most high-lift systems involve multiple airfoil elements. These systems have very high levels of total circulation, which is strongly influenced by the flow over the flap element. The flap, in turn, is influenced by the characteristics of the viscous wakes generated by the other elements. Thus a change in the transition location on one of the elements can lead to a change in the total circulation, affecting the entire flowfield.[1]

The most widely used method for estimating the transition location is the e^N method.[2,3] Some of the more recent extensions

and applications of this method are discussed in Arnal[4] and Reed et al.[5] This method tracks the growth of a family of instabilities and links the total instability amplification to the onset of transition. The disturbance growth is characterized by an N factor such that the total-amplification ratio is $A/A_0 = e^N$. Wind-tunnel and/or flight-test data are used to correlate the value of N with transition. When the e^N method is applied for flow conditions similar to the calibration data, the method can be very effective. Parameters such as surface roughness and freestream noise can be accounted for by using a variable N-factor method.[6,7] This allows the method to be applied effectively over a wider range of conditions without additional calibration.

Although the e^N method is routinely used for predicting transition, most of the applications of the method are in a "stand-alone" mode, where the stability calculations are done as a postprocessing step in a CFD computation. Integration of the method into a CFD code is hindered by the computational effort required for the stability calculations and by the stability-code demands for an accurate mean flow; the required convergence is much greater for obtaining velocity profiles than for determining lift and drag.[8] Also, the stability calculations typically require significant user interaction, making the method impractical for routine CFD application.

A number of e^N methods have been developed to help circumvent these shortcomings for CFD code integration. For two-dimensional boundary layers Drela and Giles[9] developed an N-factor equation based on the slopes of the N-factor envelopes for the family of Falkner–Skan boundary layers. This simple equation is easy to apply, and it gives reasonable results for boundary layers, which evolve slowly in the streamwise direction. In rapidly changing boundary layers the profiles are different from Falkner–Skan profiles, and the local slope of the N-factor curve also differs from the associated Falkner–Skan flow. This method, however, is not easily extended to three-dimensional boundary layers.

Another approach is to replace the stability calculations with a database of growth rates that are generated a priori for some family of profiles, typically similarity profiles. Methods of this type have been developed by Dagenhart[10] and Casalis and Arnal[11] for crossflow instabilities, and Arnal,[12] Stock and Degenhart,[13] and Gaster and Jiang[14] for Tollmien–Schlichtings (TS) waves. Each of these methods has a restricted range of applicability. Integral quantities, velocity maximums, velocity-derivative maximums, and local Reynolds numbers are used to characterize the boundary-layer mean flow. Growth rates are represented by algebraic functions of these parameters. The accuracy of these methods depends strongly on the parameters used to characterize the boundary layer and on the size, form, and generality of the database. The method of Gaster and Jiang,[14] for example, gives very accurate estimates for the growth rates but currently only for two-dimensional boundary layers. One of the critical issues when applying these methods is that the parameters used to characterize the profiles might not properly describe the general nonsimilar boundary layer.

The current method also uses a database for the growth rates, which are represented by a trained neural network based on Falkner–Skan–Cooke profiles. Neural networks have been used previously in conjunction with integral-quantity inputs to estimate growth rates for free shear-layer instabilities.[15] Here, detailed information about the velocity profiles is used instead of relying on the integral quantities.[16] Earlier attempts to use integral quantities as the bases for the neural network yielded unsatisfactory results when applied to swept-wing test cases. Neural networks are used to evaluate the growth rates for boundary-layer instabilities (namely, TS waves and crossflow instabilities) using a set of 16 inputs. The current method covers the complete range of conditions encountered in swept-wing flows.

II. *N*-Factor Formulation

Consider a three-dimensional boundary layer on a swept wing inclined at an angle Λ relative to a freestream velocity Q_∞. We introduce two coordinate systems as shown in Fig. 1. The coordinate system (x, y, z) is aligned with wing chord. The streamwise coordinate system (x_s, y, z_s) is aligned with the local edge velocity Q_e such that x_s is streamwise. The two coordinate systems are

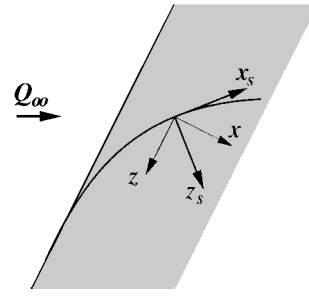

Fig. 1 Schematic of wing section showing chordwise and streamwise coordinate systems.

related by the local sweep angle ψ_e. The boundary-layer velocity corresponding to the chordwise and streamwise systems are given by (U, V, W) and (U_s, V, W_s), respectively. Within the streamwise system we define the length scales

$$\delta_1^* = \int_0^\infty \left(1 - \frac{U_s}{Q_e}\right) \mathrm{d}y, \qquad \delta_2^* = \int_0^\infty \frac{W_s}{Q_e}\, \mathrm{d}y$$

The flow is assumed to be incompressible $M_e \approx 0$ and spanwise independent $\mathrm{d}U/\mathrm{d}z = \mathrm{d}W/\mathrm{d}z = 0$. The boundary layer at each spanwise station is treated as a section of an infinite swept wing, characterized by a local sweep angle. The stability results are based on the quasi-parallel approximation.

The base flow at a given x position is represented by $[U(y; x), 0, W(y; x)]$ in the chordwise system. The linear growth of perturbations to this base flow is considered using stability theory. The form of the perturbation is given as

$$(u', v', w') = [u(y), v(y), w(y)] \exp[i(\alpha x + \beta z - \omega t)] \tag{1}$$

The perturbation velocities are governed by the Orr–Sommerfeld and Squire equations with homogeneous boundary conditions at the surface and at the outer limit of the boundary layer. These equations provide a local relationship between the (real) frequency ω, the (real) spanwise wave number β, and the (complex) chordwise wave number α for a given boundary-layer flow. Both ω and β are prescribed, and α is obtained as an eigenvalue of the Orr–Sommerfeld equation:

$$\frac{1}{R_{\delta_1^*}}\left[\frac{\mathrm{d}^4}{\mathrm{d}y^4} - 2(\alpha^2+\beta^2)\frac{\mathrm{d}^2}{\mathrm{d}y^2} + (\alpha^2+\beta^2)^2\right]v - i(\alpha U + \beta W - \omega)$$

$$\times\left(\frac{\mathrm{d}^2}{\mathrm{d}y^2} - \alpha^2 - \beta^2\right)v - i\left(\alpha\frac{\mathrm{d}^2 U}{\mathrm{d}y^2} + \beta\frac{\mathrm{d}^2 W}{\mathrm{d}y^2}\right)v = 0 \tag{2}$$

with homogeneous boundary conditions. The eigenvalue problem can be formulated in either the chordwise or the streamwise coordinate systems, but the condition that β is real applies only to the chordwise system (that is, β_s is complex).

For the stability analysis the variables are nondimensionalized by the edge velocity Q_e and the displacement thickness δ_1^* (based on the streamwise profile U_s). This yields the local Reynolds number $R_{\delta_1^*} = Q_e \delta_1^*/\nu$. For a given boundary layer the (dimensional) frequency and spanwise wave number are fixed for any physical mode. Solution of the eigenvalue problem yields the complex α at each x position. The growth rate is given by the imaginary part $-\alpha_i(\omega, \beta; x)$. The N factor for a physical mode is determined by integrating the growth rate downstream from the neutral point.

As a first application of the method, we consider an N factor based on the maximum growth over all (real) spanwise wave numbers. This leads to the definition of a maximum growth rate:

$$\gamma(\omega; x) = \max_\beta[-\alpha_i(\omega, \beta; x)] \tag{3}$$

For $\omega \neq 0$, the maximum over β is a local maximum for a given mode of instability. Thus, TS waves and traveling crossflow (CF) instabilities are treated as distinct, and the β associated with γ for a given mode changes slowly with x. Currently, only the stationary crossflow instabilities are considered. The N factor is defined as

$$N_{\mathrm{CF}}(x) = \int_{x0}^{x} \gamma(0; x)\, \mathrm{d}x \tag{4}$$

for stationary crossflow modes and

$$N_{\mathrm{TS}}(x) = \max_{\omega}\left[\int_{x_0}^{x} \gamma(\omega; x)\,\mathrm{d}x\right] \tag{5}$$

for TS waves where x_0 corresponds to the neutral-point location $\gamma(\omega; x_0) = 0$. The use of the maximum growth rate removes the β dependence from γ. This simplification results in nonphysical N factors, but these N factors provide a reasonable correlation with experiments and, thus, provide a good engineering application of the method. Transition as a result of instability is assumed to occur whenever an N factor exceeds an empirically defined threshold value (that is, $N_{\mathrm{CF}} \geq N^*_{\mathrm{CF}}$ or $N_{\mathrm{TS}} \geq N^*_{\mathrm{TS}}$).

III. Neural-Network Approach

In the calculation of the N factors, we make use of a neural network to replace the solution of the stability equation (2). Because the neural network is based on nonlinear operators, it can effectively model rather complex response surfaces in a straightforward manner.

The neural network, once trained, produces an output vector for a given input vector. This is shown schematically in Fig. 2 for an one-element output. The initial input vector provides the node outputs for the first layer of the network. The outputs of layer 1 are weighted and passed on to layer 2. For each node of layer 2, the weighted layer-1 outputs are summed to provide the node input; the input is passed through a sigmoid transfer function to generate the node output. These outputs are weighted and passed on to the next layer. The process repeats until the last-layer output provides the network output vector.

The input vector consists of scaled values of 16 variables, which are listed in Table 1. These variables are scaled to be within the range (0,1). The scaling is established from the initial training set described next. The network output is a scaled value g of the growth rate γ.

The neural network is set up to use the same basic information that feeds into the Orr–Sommerfeld eigenvalue problem. The inputs into the Orr–Sommerfeld problem include $R_{\delta_1^*}$; ω (or $F = 10^6\omega\nu/Q_e^2$); β; the profiles U_s, W_s; and the second derivatives $\mathrm{d}^2U_s/\mathrm{d}y^2$, $\mathrm{d}^2W_s/\mathrm{d}y^2$. The Reynolds number and frequency are also used as neural-network inputs. For the growth rate γ the dependence on β is removed using Eq. (3). The neural network uses the first derivative of the velocity profiles as inputs, measured at uniformly spaced locations across the boundary layer. This provides a reasonable characterization of the profiles without an excessive number of inputs. Using the actual velocity profiles, and not just integral quantities, the neural network can provide a substitute for the eigenvalue problem without forfeiting any useful information. The current characterization of the profiles is a compromise between efficiency and accuracy. Figure 3 shows the profile derivatives and the discrete points used as network inputs. These profiles correspond to a favorable pressure-gradient region of a 45-deg-sweep wing. The input points include the values at the wall and are spaced $\frac{1}{2}\delta_1^*$ apart. These points clearly capture the profile slopes at the wall, the locations of peak velocities and inflection points, and other more subtle features of the profiles. Numerical studies showed no significant improvement from including one or two additional points in the profiles; larger numbers of points were not tested.

Separate neural networks are used to model the stationary CF instabilities and the TS waves. The neural-network weights are set during a training phase. Training consists of successive adjustments of the weights in order to reduce the error between predicted and actual (scaled) growth rates for a large collection of conditions, referred to as the training set. The training set is based on Orr–Sommerfeld solutions for the Falkner–Skan–Cooke family of mean profiles. The instability growth rates for these profiles are characterized by the parameters: β_H the Hartree parameter, ψ_e the edge sweep angle, $R_{\delta_1^*}$ the local Reynolds number, and F the frequency parameter. The training set used for CF instabilities consisted of $J = 17{,}404$ different conditions spread over the parameter ranges of Table 2. The TS-wave training set had $J = 24{,}920$ different conditions over the ranges of Table 3.

Backpropagation is the training algorithm used to minimize the error $|g_j - g|$, where g_j is the network output and g is the scaled

Table 1 Neural-network input variables

Variable	Definition
$R_{\delta_1^*}$	$Q_e\delta_1^*/\nu$ Reynolds number
$R_{\delta_2^*}$	$Q_e\delta_2^*/\nu$ Reynolds number
F	$10^6\omega\nu/Q_e^2$ frequency parameter
ψ_e	$\tan^{-1}(W_e/U_e)$ stream angle
U'_{sj}	$\mathrm{d}U_s/\mathrm{d}y$ at $y/\delta_1^* = \frac{1}{2}(j-1)$, $j = 1, 6$
W'_{sj}	$\mathrm{d}W_s/\mathrm{d}y$ at $y/\delta_1^* = \frac{1}{2}(j-1)$, $j = 1, 6$

Table 2 CF training-set parameter ranges

Variable	Lower limit	Upper limit
β_H	0	1
ψ_e	5 deg	90 deg
$R_{\delta_1^*}$	150	6000
F	0	0

Table 3 TS training-set parameter ranges

Variable	Lower limit	Upper limit
β_H	−0.18	0.2
ψ_e	0 deg	60 deg
$R_{\delta_1^*}$	100	6000
F	10	90

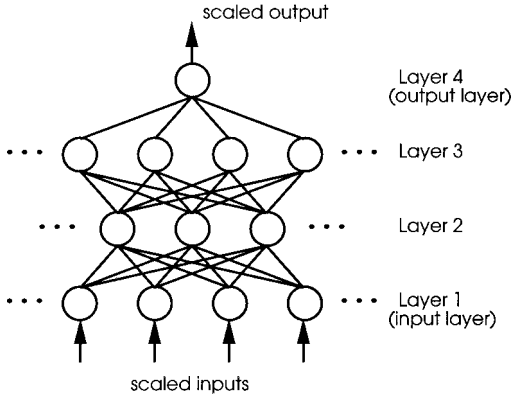

Fig. 2 Schematic of neural network used to model the stability equations.

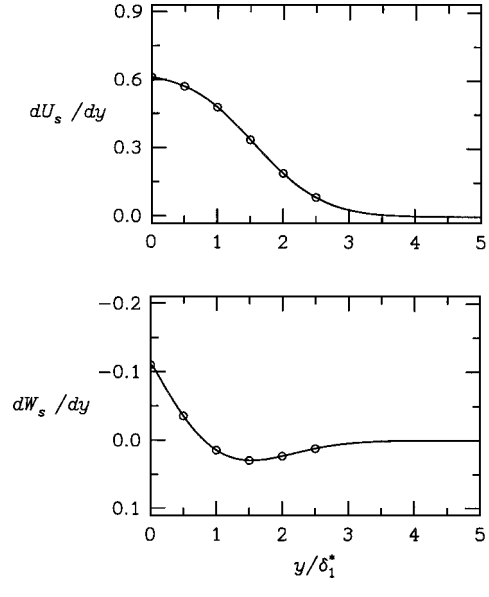

Fig. 3 Profile derivatives with symbols showing values used for network inputs.

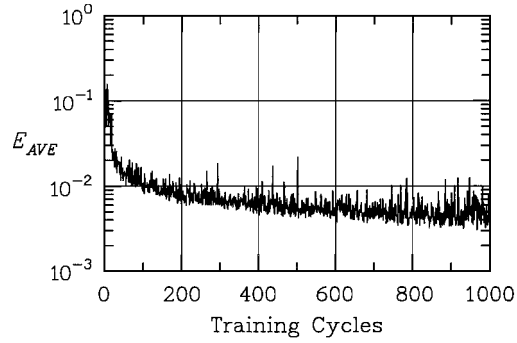

Fig. 4 CF-instability neural-network error averaged over the complete training set during the training process.

growth rate ($g = 0.40 + 15\gamma$ for CF instabilities and $g = 0.05 + 12\gamma$ for TS waves). During one training cycle, each condition in the training set is sequentially input to the network, and the weights are adjusted. The ordering of the training set is randomly shifted from one training cycle to the next to avoid biases. The average error of the network based on the entire training set

$$E_{\text{ave}} = \left(\frac{1}{J}\right) \sum_{j=1}^{J} \sqrt{(g_j - g)^2}$$

is calculated at the end of each training cycle. This quantity is plotted in Fig. 4 as a function of the number of training cycles for the training of the CF-instability network. The network is initialized with random weights, and $E_{\text{ave}} = 0.11$. After 1000 training cycles $E_{\text{ave}} \approx 0.004$. For the TS-wave network E_{ave} is initially 0.1, and after 2000 training cycles $E_{\text{ave}} \approx 0.01$. The training set covers a fairly broad range of conditions. Once the neural networks are trained, they each function as a "black box" providing the CF, $\gamma(0; x)$, and TS, $\gamma(\omega; x)$, growth rates for a given boundary-layer solution.

IV. *N*-Factor Results

The accuracy of the neural-network N factors are evaluated by comparison with Orr–Sommerfeld N-factor calculations based on the same integration strategy. Figure 5 shows the C_p distribution and the crossflow instability N factors for the experimental conditions of Reibert et al.[17] The wing sweep is $\Lambda = 45$ deg. The C_p shows a favorable gradient over the region of interest. The N factors increase monotonically, and the methods show the same trend with Reynolds number. Differences between the neural-network and Orr–Sommerfeld N factors are less than one. This is within the range of N-factor scatter for typical correlations with transition.

Results for a slightly more complex C_p distribution are shown in Fig. 6. For this case the favorable gradient is interrupted by a region of flat and mildly adverse pressure gradient. The sweep angle is $\Lambda = 35$ deg, and three Reynolds numbers are considered. The N-factor results show very good agreement (again, the differences are less than one), especially at the higher Reynolds numbers. At lower Reynolds numbers the neural network shows a consistent overprediction of the growth rate near the neutral point.

We now consider TS waves, which are a primary source for transition in adverse pressure gradients. The TS-wave growth rates are found to show an exaggerated sensitivity to S-shaped crossflow profiles, which often occur just downstream of the pressure minimum. This sensitivity stems from the fact that no S-shaped profiles were used in the network training. Hence, in the neural-network evaluation of the TS-wave growth rates the crossflow velocity profile is not used. Neglecting the crossflow profile does have some adverse effects on the estimated growth rates further downstream. However, the only other alternative is to use a different profile family for training the neural network.

Figure 7 shows the C_p distribution and the TS wave N factor for a wing with a mild sweep of $\Lambda = 10$ deg. At this Reynolds number the N factor shows growth soon after the start of the adverse gradient. The two methods are in reasonable agreement, with differences less than $\Delta N_{\text{TS}} = 1$. The primary differences in the growth rate occur just downstream of the neutral point.

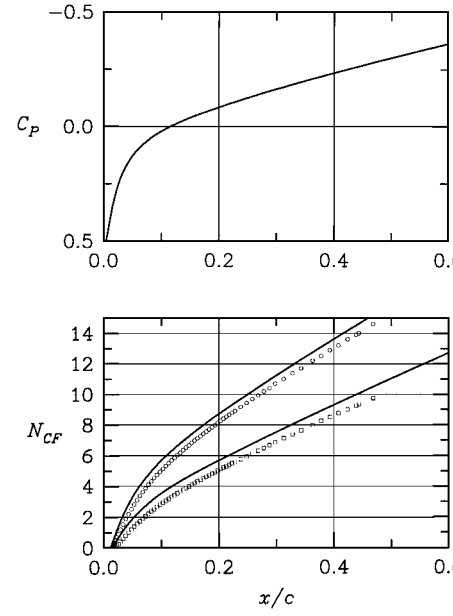

Fig. 5 C_p distribution and CF instability N factors. Comparison to Orr–Sommerfeld calculations (symbols) for the conditions $\Lambda = 45$ deg: □, $R_c = 3.2 \times 10^6$; and ○, $R_c = 5 \times 10^6$.

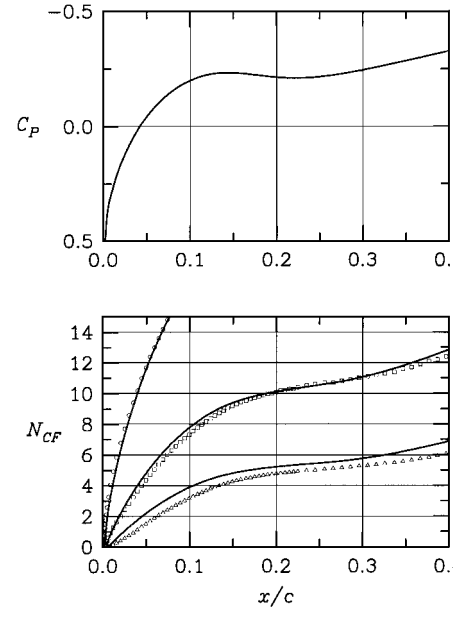

Fig. 6 C_p distribution and CF instability N factors. Comparison to Orr–Sommerfeld calculations (symbols) for the conditions $\Lambda = 35$-deg: △, $R_c = 5 \times 10^6$; □, $R_c = 10 \times 10^6$; and ○, $R_c = 25 \times 10^6$.

A more complicated case for TS-wave N factors is given in Fig. 8. The wing sweep is $\Lambda = 36$ deg. In this case the adverse pressure gradient diminishes downstream of the peak, leading to stabilization of the boundary layer at lower Reynolds numbers. This trend is captured in the neural-network results. Figure 8 shows reasonable agreement between the two methods, but the neural-network N factors are sometimes larger, and sometimes smaller, than the Orr–Sommerfeld results. Some of these differences are the result of neglecting the crossflow profiles when evaluating the TS-wave growth rates (as already discussed).

A final comparison for TS waves is given in Fig. 9. Results are given for a sweep angle of $\Lambda = 45$ deg at three Reynolds numbers. These results show greater differences than the other cases, but the maximum differences are still close to $\Delta N_{\text{TS}} \approx 1$.

In general, the differences between the neural-network and the Orr–Sommerfeld N factors are greater for TS waves as compared to crossflow vortices. This was observed for a wider range of conditions than is shown here. The primary source of error in the neural-network growth rates stems from the use of the Falkner–Skan–Cooke

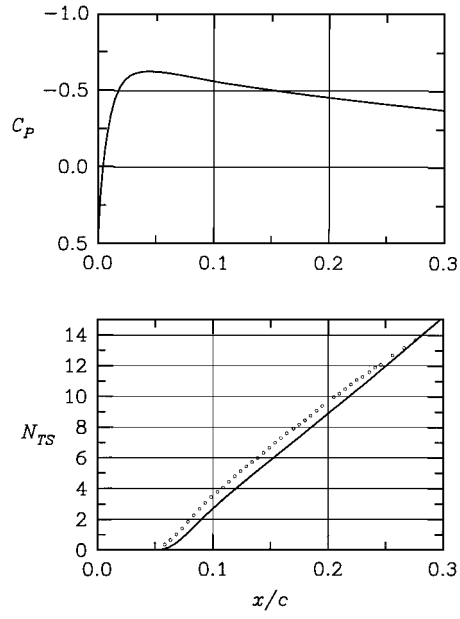

Fig. 7 C_p **distribution and TS instability** N **factor. Comparison to Orr–Sommerfeld calculations (symbols) for the conditions** $\Lambda = 10$ **deg and** $R_c = 5 \times 10^6$.

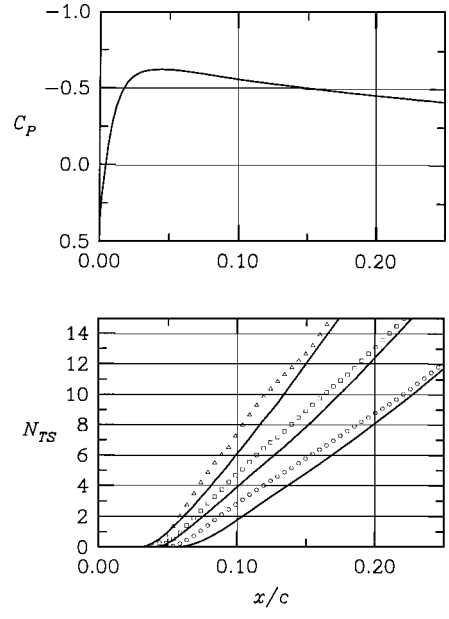

Fig. 9 C_p **distribution and TS instability** N **factors. Comparison to Orr–Sommerfeld calculations (symbols) for the conditions** $\Lambda = 45$**-deg: ○,** $R_c = 4 \times 10^6$**; □,** $R_c = 8 \times 10^6$**; and △,** $R_c = 16 \times 10^6$.

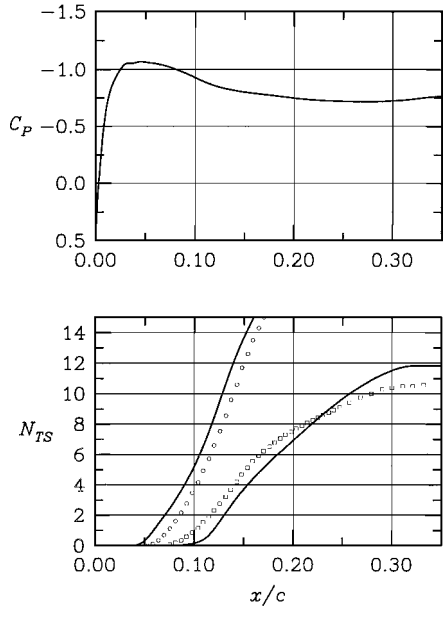

Fig. 8 C_p **distribution and TS instability** N **factor. Comparison to Orr–Sommerfeld calculations (symbols) for the conditions** $\Lambda = 36$ **deg: □,** $R_c = 1.4 \times 10^6$**; and○,** $R_c = 5.8 \times 10^6$.

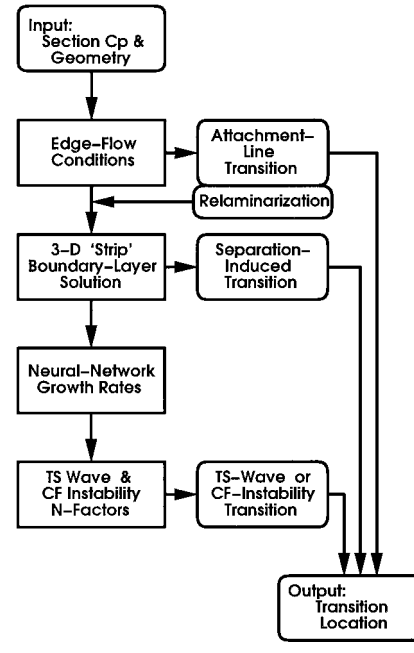

Fig. 10 Flow diagram for estimating transition location.

(FSC) family of profiles for training the network. Boundary layers that develop in changing pressure gradients exhibit features that are not present in the FSC profiles. Even though the network uses the actual velocity profiles as inputs, when these profiles differ significantly from the training-set profiles the network can only approximate the true value.

The translation of the N-factor error to increased uncertainty in the transition location will depend on the slope of the N-factor curve at the transition point $(\mathrm{d}N/\mathrm{d}x)|_{N=N^*}$. The steeper the slope, the smaller the uncertainty in the estimated transition locations. For a transition N factor of, e.g., $N^* = 10$, an N-factor error of 1 will result in roughly a 10% error in the estimated extent of laminar flow, assuming the transition N factor N^* is perfectly correlated with the occurrence of transition. In practice, there are uncertainties in the transition N factor N^* that depend on the fidelity of the empirical correlation. Even for the best cases, the variation of the correlated N^* is approximately 1 (Ref. 7), and so the N-factor errors associated with the current method are not expected to be significant.

V. Estimating the Transition Location

There are several mechanisms by which a boundary layer on a swept wing can become turbulent. (For example, turbulence can enter the boundary layer along the attachment line, thus providing a "contamination" of the laminar flow; the boundary layer can undergo laminar separation followed by shear-layer transition leading to a separation bubble; or the laminar boundary layer can undergo a "natural" transition caused by instability.) Each of these mechanisms must be accounted for in determining the location for "tripping the boundary layer" in CFD codes. Figure 10 shows a method for estimating the transition location, which makes use of the neural network for modeling the instability growth. This scheme accounts for the attachment-line state, for separation, and for instability.

The attachment-line state depends on the inviscid parameter $\bar{R} = W_e/\sqrt{(\nu\, \mathrm{d}U_e/\mathrm{d}x|_{x=0})}$ (for example, see Refs. 18–21). For $\bar{R} \leq 245$, the attachment line is considered to be laminar. When $245 < \bar{R} < 580$, the attachment-line state depends on the inflow conditions. Above $\bar{R} = 580$ the attachment line is unstable and

is taken to be turbulent. The relaminarization parameter $K = (\nu/Q_e^2)\,\mathrm{d}Q_e/\mathrm{d}x_s$ is evaluated if the attachment line is turbulent. Absent any swept-wing relaminarization criteria, the boundary layer is assumed to relaminarize if $K_{\max} \geq 3(10)^{-6}$. This value is based on two-dimensional flat-plate experiments.[22] More recent studies support the use of the flat-plate data for predicting relaminarization in flows of practical interest.[23,24] The TS-wave N factor at transition N^*_{TS} used for a relaminarized boundary layer is significantly smaller than that for fully laminar boundary layers due to the high residual disturbance levels.[24]

For laminar or relaminarized boundary layers, an infinite-sweep strip boundary layer is calculated using a finite difference scheme. If laminar separation is encountered, the flow is assumed to begin transition at the separation point. This provides a crude approximation for a laminar separation bubble. The effective bubble length will be determined by a turbulence model. Improved modeling can be accommodated in future versions of this scheme.

The laminar boundary-layer solution is used to generate the neural-network inputs at each chordwise station (that is, the variables of Table 1). The neural-network growth rates are integrated according to Eqs. (4) and (5) to obtain the N factors $N_{\mathrm{CF}}(x)$ and $N_{\mathrm{TS}}(x)$, respectively. Transition caused by instability is assumed to occur whenever the calculated N factors reach the empirically defined transition values, denoted N^*_{CF} and N^*_{TS}. The values for N^*_{CF} and N^*_{TS} used here will differ somewhat from the N-factor values based on growth-curve envelopes of purely physical modes.

The scheme described by Fig. 10 serves as the basis for a simple transition-prediction subroutine (XTran). The inputs/outputs for the subroutine are based on a wing cut aligned with the freestream velocity Q_∞. The primary subroutine inputs are

$$(X/C)_i,\ (Y/C)_i,\ (C_p)_i,\ R_C,\ M_\infty,\ \Lambda$$

The variable X corresponds to the freestream velocity direction, and the variable Y is perpendicular to X such that the wing section is described by a set of points (X_i, Y_i), $i = 1, i_{\max}$. C_{p_i} are the values of the C_p at the points (X_i, Y_i), $i = 1, i_{\max}$. All quantities are nondimensionalized by the reference chord C and the velocity Q_∞. Thus the chord Reynolds number is defined by $R_C = Q_\infty C/\nu$. The freestream Mach number M_∞ is only used to calculate the edge velocities from the given C_p distribution. The leading-edge geometric sweep Λ is used to transform the streamwise section cut (in the X direction) into a chordwise cut (in the x direction).

The primary outputs of the routine are

$$(X/C)_{\mathrm{Tran}},\ (Y/C)_{\mathrm{Tran}},\ \mathrm{mode}$$

The transition location is given by the coordinates $(X/C)_{\mathrm{Tran}}$, $(Y/C)_{\mathrm{Tran}}$. The variable mode is used to describe the mechanism of transition: attachment-line transition, transition at laminar separation, transition caused by crossflow instability, and transition caused by TS waves. The estimated transition location corresponds to the transition onset.

VI. Conclusions

A method has been developed for estimating the transition location in CFD codes. This method accounts for the primary transition mechanisms associated with three-dimensional swept-wing boundary layers, including attachment-line transition, crossflow instability, Tollmien–Schlichting instability, and transition triggered by separation. The e^N method is used to predict transition caused by crossflow and TS-wave instabilities. A neural-network method is used to provide the growth rates for calculating the N factors.

The method assumes that the flow is incompressible and is, therefore, limited to lower Mach numbers. The stability analysis, underlying the neural-network growth rates, assumes an infinite-sweep boundary layer subject to the quasi-parallel-flow approximation. The N factors are based on the integral of the fixed-frequency growth rates maximized over the (real) spanwise wave number. Calculations show the neural-network and Orr–Sommerfeld results are in good agreement over a practical range of flow conditions. The neural-network approach is several hundred times faster than solving the full stability equations, and it is robust enough that it requires no user intervention. This allows the approach to be directly coupled with CFD codes.

A transition-prediction subroutine has been developed based on the neural-network modeling. The inputs required are easily obtained from a CFD code. The subroutine outputs the transition location and an indication of the mechanism responsible for causing transition. Future efforts will focus on improved physical modeling and on calibration of the current model, including application studies.

References

[1]Kusunose, K., Wigton, L., and Meredith, P., "A Rapidly Converging Viscous/Inviscid Coupling Code for Multi-Element Airfoil Configurations," AIAA Paper 91-0177, Jan. 1991.

[2]Smith, A. M. O., and Gamberoni, A. H., "Transition, Pressure Gradient and Stability Theory," Douglas Aircraft Co., Rept. ES26388, El Segundo, CA, 1956.

[3]Van Ingen, J. L., "A Suggested Semi-Empirical Method for the Calculation of the Boundary Layer Transition Region," Univ. of Technology, Rept. UTH1-74, Delft, The Netherlands, 1956.

[4]Arnal, D., "Boundary Layer Transition: Predictions Based on Linear Theory," R 793, AGARD, Paper 2, March 1993.

[5]Reed, H. L., Saric, W. S., and Arnal, D., "Linear Stability Theory Applied to Boundary Layers," *Annual Review of Fluid Mechanics*, Vol. 28, 1996, pp. 389–428.

[6]Mack, L. M., "Transition Prediction and Linear Stability Theory," *Laminar-Turbulent Transition*, CP 224, AGARD, 1977, pp. 1/1–22.

[7]Crouch, J. D., and Ng, L. L., "Variable N-Factor Method for Transition Prediction in Three-Dimensional Boundary Layers," *AIAA Journal*, Vol. 38, No. 2, 2000, pp. 211–216.

[8]Stock, H. W., and Haase, W., "Feasibility Study of e^N Transition Prediction in Navier–Stokes Methods for Airfoils," *AIAA Journal*, Vol. 37, No. 10, 1999, pp. 1187–1196.

[9]Drela, M., and Giles, M. B., "Viscous-Inviscid Analysis of Transonic and Low Reynolds Number Airfoils," AIAA Paper 86-1786, 1986.

[10]Dagenhart, J. R., "Amplified Crossflow Disturbances in the Laminar Layer on Swept Wings with Suction," NASA TP-1902, Nov. 1981.

[11]Casalis, G., and Arnal, D., "ELFIN II, Subtask 2.3: Development and Validation of a Simplified Method for Pure Crossflow Instability at Low Speed," ONERA, TR 145, Toulouse, France, Dec. 1996.

[12]Arnal, D., "Transition Prediction in Transonic Flow," *Symposium Transsonicum III*, Springer-Verlag, Berlin, 1989, pp. 253–262.

[13]Stock, H. W., and Degenhart, E., "A Simplified e^n Method for Transition Prediction in Two-Dimensional, Incompressible Boundary Layers," *Zeitschrift für Flugwissenschaften Weltraumforsch.*, Vol. 13, 1989, pp. 16–30.

[14]Gaster, M., and Jiang, F., "Rapid Scheme for Estimating Transition on Wings by Linear Stability Theory," *ICAS International Council of the Aeronautical Sciences Proceedings*, Vol. 3, Anaheim, CA, 1995, pp. 1104–1113.

[15]Fuller, R., Saunders, W., and Vandsburger, U., "Neural Network Estimation of Disturbance Growth Using a Linear Stability Numerical Model," AIAA Paper 97-0559, Jan. 1997.

[16]Crouch, J. D., Crouch, I. W. M., and Ng, L. L., "Estimating the Laminar/Turbulent Transition Location in Three-Dimensional Boundary Layers for CFD Applications," Boeing Co., Rept. D6-82448, Seattle, WA, May 1999.

[17]Reibert, M. S., Saric, W. S., Carrillo, R. B., and Chapman, K. L., "Experiments in Nonlinear Saturation of Stationary Crossflow Vortices in a Swept-Wing Boundary Layer," AIAA Paper 96-0184, Jan. 1996.

[18]Gaster, M., "On the Flow Along Swept Leading Edges," *Aeronautical Quarterly*, Vol. 18, 1967, pp. 165–184.

[19]Poll, D. I. A., "Transition in the Infinite Swept Attachment-Line Boundary Layer," *Aeronautical Quarterly*, Vol. 30, 1979, pp. 607–629.

[20]Spalart, P. R., "Direct Numerical Study of Leading-Edge Contamination," *Fluid Dynamics of Three-Dimensional Turbulent Shear Flow and Transition*, CP 438, AGARD, 1988, pp. 5/1–12.

[21]Arnal, D., and Juillen, J. C., "Leading-Edge Contamination and Relaminarization on a Swept Wing at Incidence," *Proceedings of the Numerical and Physical Aspects of Aerodynamic Flows IV*, Springer-Verlag, Berlin, 1990, pp. 391–402.

[22]Launder, B. E., "Laminarization of the Turbulent Boundary Layer by Acceleration," Gas Turbine Lab., Rept. 77, Massachusetts Inst. of Technology, Cambridge, MA, 1964.

[23]van Dam, C. P., Los, S. M., Miley, S. J., Roback, V. E., Yip, L. P., Bertelrud, P. M., and Vijgen, P. M. H. W., "In-Flight Boundary-Layer State Measurements on a High-Lift System: Slat," *Journal of Aircraft*, Vol. 34, No. 6, 1997, pp. 748–756.

[24]Mukund, R., Viswanath, P. R., and Crouch, J. D., "Relaminarization and Retransition of Accelerated Turbulent Boundary Layers on a Convex Surface," *Laminar–Turbulent Transition*, Springer-Verlag, Berlin, 2000, pp. 243–248.

P. J. Morris
Associate Editor